Nickel–molybdenum catalysts for combined solid oxide fuel cell internal steam and dry reforming

Majewski, Artur; Singh, Sunit K. ; Labhasetwar, Nitin K. ; Steinberger-Wilckens, Robert

DOI:
10.1016/j.ces.2020.116341

Nickel–molybdenum catalysts for combined solid oxide fuel cells internal steam and dry reforming

Artur J. Majewski (1)*, Sunit K. Singh (2), Nitin K. Labhasetwar (2), Robert Steinberger-Wilckens (1)

(1) School of Chemical Engineering, University of Birmingham, B15 2TT, UK

(2) Energy and Resource Management Division, CSIR-National Environmental Engineering Research Institute (NEERI), Nehru Marg, Nagpur - 440 020, India

* a.j.majewski@bham.ac.uk

Abstract

A series of supported Ni-Mo catalysts were synthesised through a deposition-co-precipitation method (DcP) and investigated in combined steam and dry reforming. The morphology of the oxide precursors and reduced catalysts and their composition were determined via XRF, TEM, SEM, TGA, TPR, BET, and XRD. The prepared Ni-Mo catalysts supported by Yttria-Stabilised Zirconia (YSZ), Gadolinium-Doped Ceria (GDC) and Ceria Stabilised Zirconia (CSZ) with improved carbon tolerance have the potential to be used as anodes in Solid Oxide Fuel Cells (SOFC). The application of those catalysts is for the anode supporting layer where most of the internal reforming reaction takes place. Those catalysts were compared to conventional reforming catalysts with Al_2O_3 and TiO_2 supports typical for reforming catalysts. The performance for Ni-Mo catalysts according to the support materials was observed in the sequence Al_2O_3 > YSZ > TiO_2 > CSZ > GDC. Formation of MoC_2 improved catalytic activity towards steam reforming reaction. Increasing the Mo loading to Ni catalyst improved the coke resistance properties, however, reduced the catalytic activity. The N-Mo/YSZ catalyst presented stable performance during 100 hours of combined steam and dry reforming.

Keywords: Ni-Mo catalyst, combined steam and dry reforming, molybdenum carbide

Introduction

Hydrogen produced from biogas is one of the options to supply ‘green’ zero-carbon hydrogen from renewable sources. Efficient hydrogen production by biogas reforming requires a catalyst to minimise the kinetic barriers imposed by the activation energy for the formation of the reaction intermediates on the catalyst surface. The most common catalysts used for combined steam and dry reforming reactions and hydrogen production are based on Ni owing to its high activity and low cost. Reforming catalysts are usually composed of Ni supported on porous support materials.

Many reports confirmed that the performance of Solid Oxide Fuel Cells (SOFC) with internal combined steam and dry reforming of CH_4 is 20 to 70% lower than SOFC with H_2 as a fuel (Hua et al., 2016b; Lanzini and Leone, 2010; Rismanchian et al., 2015). Adjusting reforming conditions and the application of highly active reforming catalysts are cost-effective methods to solve issues with combined steam and dry reforming. The presence of molybdenum in a Ni-based catalyst can influence catalyst selectivity and efficiency toward a number of reactions (Asset et al., 2016). A combination of the two metals results in an enhanced catalyst activity (Fang et al., 2016). Ni-Mo catalysts are applied for hydrotreating reactions in petroleum refining processes and especially in the removal of sulphur (Behnejad et al., 2019; Liu et al., 2014), hydrodenitrogenation (Behnejad et al., 2019) and thioetherification (Shen et al., 2019). Using Mo as a promoter for Ni-based catalysts for reforming of CH_4 (Sehested et al., 2001; Xiong et al., 2015; Yao et al., 2017), toluene (Claude et al., 2020) or liquid hydrocarbons (Bkour et al., 2020) has also been reported. A Mo-rich catalyst can be effective in hydrodesulphurisation (Liu et al., 2015). Amorphous Ni-Mo nanopowders synthesised by reduction of Ni-Mo oxides have been

reported to have much-improved activity compared to pure Ni catalysts (McKone et al., 2013). For the Ni-Mo bimetallic catalysts, two solid solutions can be formed: one being Ni-rich and the other Mo-rich. The increase in Ni-rich phase enhances the catalyst's activity and the Mo phase stabilises the catalyst (Asset et al., 2016; Hua et al., 2016a; Maluf and Assaf, 2009). The addition of Mo in a catalyst can improve performance for sulphur-containing fuel gases due to the formation of a NiMoS phase (Liu et al., 2015). For Ni-Mo catalysts, lowering the reduction and pre-treatment temperature improves activity and the formation of the less active $MoNi_4$ phase is avoided (Yao et al., 2017). The hydrodesulphurisation properties of these catalysts can find application in reforming of biogas and natural gas which both can have sulphur impurities. This is an attractive option for internal reforming in SOFCs.

SOFCs are highly efficient energy converters for hydrogen and hydrocarbon fuels. Nevertheless, potential coke formation when operating on hydrocarbons still calls for research on novel anodes that are less prone to carbon deposition. Deposition-co-precipitation of Mo on Ni-based catalysts and formation of binary and ternary nanoparticle cermets improves anode performance (Niakolas et al., 2013; Niakolas et al., 2011). The deposition-co-precipitation method also results in the formation of more stable Ni-Mo catalyst structures than mechanical mixing, which is a common method in SOFC anode fabrication (Shi et al., 2012). (Ma et al., 2014) observed that high metal loading resulted in catalyst deactivation due to Ni sintering for Ni-Mo catalysts during steam reforming. Although aqueous impregnation methods with additional nanoscale catalysts (McIntosh et al., 2003; Troskialina et al., 2015) showed to be effective in carbon deposition reduction, they still need verification to confirm long-term stability due to the common tendency of nanosized particles to agglomerate at high temperatures. An alternative is the introduction of dispersed nanoparticles during anode preparation, for example, by a deposition-precipitation method.

Deposition-precipitation has many advantages for catalyst synthesis such as strong metal-support interaction, increased surface area, and the possibility to increase the amount of metal loading (Majewski et al., 2013). Introducing carbon to transition metal lattices by the formation of carbides (such as Mo_2C) may affect electronic negativity and improve the desired catalytic properties (Ma et al., 2017). Bulk molybdenum carbide itself is catalytically active in hydrogen production reactions, but supported metal/Mo carbides show higher catalytic activity (Ma et al., 2017). Pure Mo_2C is not active in dry reforming (Shi et al., 2012). However, supported Mo_2C has an activity similar to noble metals in the sequence Ru>Rh>Mo_2C>Pd>Pt (Yao et al., 2018). Introduction of Mo-carbide to the anode structure can improve the stability owing to a high melting point, and by mitigating atom mobility at elevated temperatures owing to an increase in lattice distortion (Hua et al., 2016a). It was reported (Lin et al., 2007) that supported Mo_2C catalysts are much more active than the unsupported structure. Therefore, there is scope for further improvement in the performance of Ni-Mo supported catalysts by manipulating their aggregation, for example, by using a variety of supports.

1. Scientific Approach

This study focuses on the synthesis of supported Ni-Mo catalysts and the analysis of the effect of support and Mo addition on the catalyst morphology and performances in combined steam and dry reforming. In this paper, we demonstrate the fabrication of nickel-molybdenum nanoparticle arrays on a range of supports. To explore whether such compounds are effective as combined steam and dry reforming catalysts, a series of nickel-molybdenum compositions were synthesised by deposition-co-precipitation and evaluated for reforming reactions. The proposed approach allows the provision of high dispersion of the catalyst on the support surface. Attention was given to the effect of Mo_2C formation on catalyst activity and influence of support and Ni:Mo molar proportions on the

catalytic performance. The goal was to develop a catalyst that could be introduced to the support layer of a SOFC fuel electrode to improve coke resistance during combined internal reforming of CH_4.

2. Experimental Procedures

The thermogravimetric analysis (TGA) of temperature-dependent mass change profiles was performed using a thermogravimetric analyser Netzsch 209F1. The sample mass was 10 to 20 mg. The heating rate was 5°C min^{-1} in a 5%H_2/N_2 gas mixture at a flow rate of 35 ml min^{-1}, carried out between room temperature and 1000°C for temperature-programmed reduction (TPR). Samples of a used catalyst (10 to 20 mg) were examined by temperature-programmed oxidation (TPO) to detect carbon deposition; the air flow used was 50 ml min^{-1}. The BET surface area was determined by N_2 adsorption-desorption isotherms on a Micromeritics TriStar II Plus. Samples were degassed at 200°C before the test. The structure of the catalyst was analysed by X-ray powder diffraction (XRD) using a Bruker D8 Advance. Analyses were carried out at room temperature in the 2θ range from 20 to 70°. Scanning speed was 2.2°·min^{-1} for all samples. The chemical composition of the catalysts was investigated using X-ray fluorescence spectrometry (XRF) on a Bruker S8 Tiger. For analysis, 0.5 g of each sample was ground and placed in 8 mm sample cups with a 2 µm Mylar film. The morphological properties of the tested catalysts and supports were measured using a Scanning Electron Microscope (SEM) Philips Xl-30; the accelerating voltage was 15 to 20 kV. Particle morphology was examined by transmission electron microscopy (TEM) with a JEOL TEM-2100. Samples were suspended in ethanol by sonication and deposited on a copper microgrid with a carbon film.

2.1 Preparation of nickel-molybdenum catalysts

The supported binary Ni-Mo catalysts were synthesised using a deposition-co-precipitation procedure on commercial support powders:

- **YSZ** - Yttria-Stabilised Zirconia - TOSOH corporation; 8 mole% Y,
- **GDC** - Gadolinium-Doped Ceria - Fuel Cell Materials; 10 mole% Gd,
- **Al_2O_3** - Polymer Innovations Inc,
- **TiO_2** - Sigma-Aldrich,
- **CSZ** - Ceria Stabilised Zirconia - United Ceramics Limited, 14 mole% Ce).

To compare the typical reforming catalyst supports Al_2O_3 and TiO_2 with available SOFC materials YSZ, GDC and CSZ, samples were selected with a similar surface area of around 10 m^2g^{-1}. The porosity of all the selected supports was relatively low for the typical reforming catalyst application. However, porosity was further introduced by subsequent reduction and by the addition of sacrificial pore-forming agents in case of the catalysts for SOFC anodes. All selected supports were pre-treated at 800°C (in air, 5 h) to eliminate impurities. The pre-treatment affected the support structure, reducing the surface area (especially for GDC). Use of YSZ, GDC and CSZ as support materials for the reforming catalysts opens up the possibility to develop highly active SOFC anodes that can avoid carbon deposition by promoting carbon oxidation.

Aqueous solutions of the Ni and Mo precursors, i.e. $Ni(NO_3)_2{\cdot}6H_2O$) and $(NH_4)_6Mo_7O_{24}{\cdot}4H_2O$, were mixed with a support. Different mixtures of Ni and Mo were prepared and labelled catalyst 1 through 9. The Ni-Mo nitrate solution had a molar proportion of Ni:Mo 2.3:1 for catalysts 1 to 5 and 9 (Ni-Mo precipitate), 3.4:1 for catalysts 6, 4.7:1 for catalyst 7, and catalyst 8, the Ni:Mo molar ratio was 0.3:1. The compositions are shown in Table 1. Urea was added as a reducing agent to the suspension, that was held for 4 h at 95°C leading to the precipitation of a green, mixed Ni−Mo oxide. The step was repeated to obtain 10 to 15wt% metallic loading of the active metals. After eliminating anions by washing with water, catalyst samples were dried and calcined at 800°C in air for 5 h.

This step was followed by 1 h heat-treatment (temperature-programmed reduction, TPR) to reduce the metal oxides at 750°C (under an atmosphere of H_2:CH_4:N_2 molar ratio 50:25:25). This completed the metal precursor reduction and eliminated their ligands. The catalyst reduction combined with carburisation is a complex process. During the solid-gas reaction, H_2 acts as the reducing agent for the deposited Ni and Mo oxides, while CH_4 is the carbon source for carbide formation (deposited in the same step). Ni-Mo-C structures are dense with a low specific surface area (Ma et al., 2017). Additionally, Hirose et al. (Hirose et al., 2011) reported that with the increase in temperature of catalyst pre-treatment the surface area of the Ni-Mo bulk decreased. Therefore, it was important to select a support material and deposition technique that allowed high dispersion of the active phase on the support surface with nanosized particles, while also maintaining the support micro surface area.

2.2 Characterisation of the nickel-molybdenum catalysts

The addition of a metal phase on the surface of the supporting substrates created heterogeneity and increased roughness owing to the deposition of nanoparticles, thereby increasing the surface area for the catalysts supported by YSZ, Al_2O_3 and CSZ. However, the surface area for TiO_2 and GDC catalyst precursors slightly decreased after the metal loading. This suggests that Ni-Mo co-deposition blocked some pores and the dispersion of deposited particles was lower.

Table 1. Structural parameters of the synthesised Ni-Mo catalysts (after reduction).

No	Catalyst	XRF [%]		BET [m^2g^{-1}]
		Ni	Mo	
1	13Ni-7Mo/YSZ	13.7	7.6	7.4
2	13Ni-7Mo/GDC	13.1	6.2	9.2
3	13Ni-7Mo/Al_2O_3	12.5	7.8	10.4
4	13Ni-7Mo/TiO_2	12.1	6.8	9.3
5	13Ni-7Mo/CSZ	12.3	6.6	5.4
6	23Ni-7Mo/YSZ	22.7	6.3	7.1
7	13Ni-3.5Mo/YSZ	13.5	3.5	6.2
8	13Ni-16Mo/YSZ	12.2	15.4	5.8
9	13Ni-7Mo precipitate	65.1*	34.4*	--

*dried overnight at 105°C (not calcined, not reduced).

According to XRF analyses (excluding oxygen), the loading of Ni and Mo was close to the nominal (Table 1). Increasing Ni content from 13% to 23% (with a constant 7% Mo) did not significantly affect the catalyst surface area (decrease from 7.4 to 7.1 m^2g^{-1} for catalyst 6). That is contrary to what (Nagai et al., 2006) reported, which was that for Ni-Mo catalysts increasing Ni loading decreased the catalyst surface area. However, they tested unsupported catalysts with lower Ni content than used in this work. In contrast, increasing the amount of Mo by 50%, with constant Ni loading for YSZ supported Ni-Mo precursors, increased the surface area from around 6.2 m^2g^{-1} (for 13Ni-**3.5Mo**/YSZ - catalyst 7) to 7.4 (for 13Ni-**7Mo**/YSZ - catalyst 1). Further addition of Mo, with unchanged Ni content, reduced the area by about 20% down to 5.8 m^2g^{-1} for 13Ni-**16Mo**/YSZ (catalyst 8). This can be attributed to blocked pores of the support or the formation of bigger particles (Mo-rich phase). A similar effect was reported for Ni-Mo/Al_2O_3 catalysts in (Yao et al., 2017). Usually, a nominal loading of the added metal element above 20% can cause a decrease in the catalyst surface area by blocking support porosity. This suggests that the catalyst surface area depends on the Ni:Mo proportions.

According to the Ni-Mo binary phase diagram (Wang et al., 2005), there are three known compounds at the operating temperature of 750°C depending on Ni-Mo proportion: Ni_4Mo

(for catalysts 6 and 7), Ni_3Mo (catalysts 1 to 5) and NiMo (catalyst 8). The ionic radii of Ni and Mo are close; therefore, some solubility is expected because the solvent and solute atoms are similar in atomic size. The formation of the Ni-Mo solid solution will slightly expand the Ni lattice because of the larger Mo atoms. The obtained catalysts 1 to 5 and 8 have Mo concentrations above the limit for Mo solubility (27%) in metallic Ni-Mo solid solution (Wang et al., 2005). Partial oxidation of the surface Ni atoms was reported for the Ni-Mo/YSZ structures due to the interaction between surface Ni and Mo atoms (Bkour et al., 2020). Additionally, the crystal structure of Ni and Mo is different **(**Mo body-centred cubic, Ni cubic close-packed) with different lattice parameters. Therefore, depending on the Ni:Mo molar ratio, it is possible to prepare compounds that might have novel catalytic properties.

2.3 Catalytic evaluation - oxide catalyst precursors

The reducibility of 13Ni-7Mo catalyst precursors in H_2 flow is presented in Fig. 1a for YSZ support, Fig. 1b for GDC, Fig. 1c for Al_2O_3, Fig. 1d for TiO_2 and Fig. 1e for CSZ. The tested support materials were stable at the tested temperature and the reducing atmosphere. Only the GDC and CSZ showed a small mass decrease (0.8% and 0.4%, respectively) at the temperature above 500°C, related to Ce reduction. The DTG curves of all the Ni-Mo/supported catalyst precursors showed two endothermic peaks during reduction. Both observed mass-reduction peaks were attributed to the reduction of Ni-Mo oxides. The first reduction peak was attributed to the reduction of oxides NiO and MoO_3 (either bulk and/or nanoparticles), which have a weak interaction with the support. The second peak was attributed to oxides that interacted strongly with the support and/or larger bulk particles.

The DTG curve showed a strong peak at 539°C, and a weaker peak at 732°C for the Al_2O_3 supported catalyst (Fig. 1c). The curves of the GDC and CSZ supported catalyst precursors (Fig. 1b and 1e) were similar to the 13Ni-7Mo/Al_2O_3 precursor. However, for the YSZ supported catalyst, the maximum reduction temperature was lower with 508°C for the first intensive peak and 668°C for the second peak (Fig. 1a). This suggested a lower interaction with the YSZ support. The reduction temperature observed was more than 80°C higher than the temperature reported in the literature for unsupported Ni-Mo precipitates (Liu et al., 2015). The DTG curve of the 13Ni-7Mo/TiO_2 catalyst precursor was different. The intensity of the peak at 650°C was higher than that at 479°C, with weight losses of 1.9% and 2.7%, respectively (Fig. 1d). The TiO_2 supported catalyst required higher reduction temperature, suggesting the formation of bigger particles more difficult to reduce; which was confirmed by the decrease in the BET surface area after Ni-Mo loading. For the Ni-Mo/GDC**,** the peaks were very similar to those of YSZ supports, the second being at 669°C; however, above that temperature, the catalyst mass decreased by further 0.9%, indicating poor thermal stability. The tested catalysts with cerium in the support structure were unstable in reducing atmosphere. Only a small amount of CeO_2 could be reduced at the tested reaction conditions (Kundakovic and Flytzani-Stephanopoulos, 1998). TPR results showed that the presence of Ni-Mo alloys enhanced the ceria reducibility. However, the partially reduced ceria was reported to improve catalyst coking resistance (Papaefthimiou et al., 2013).

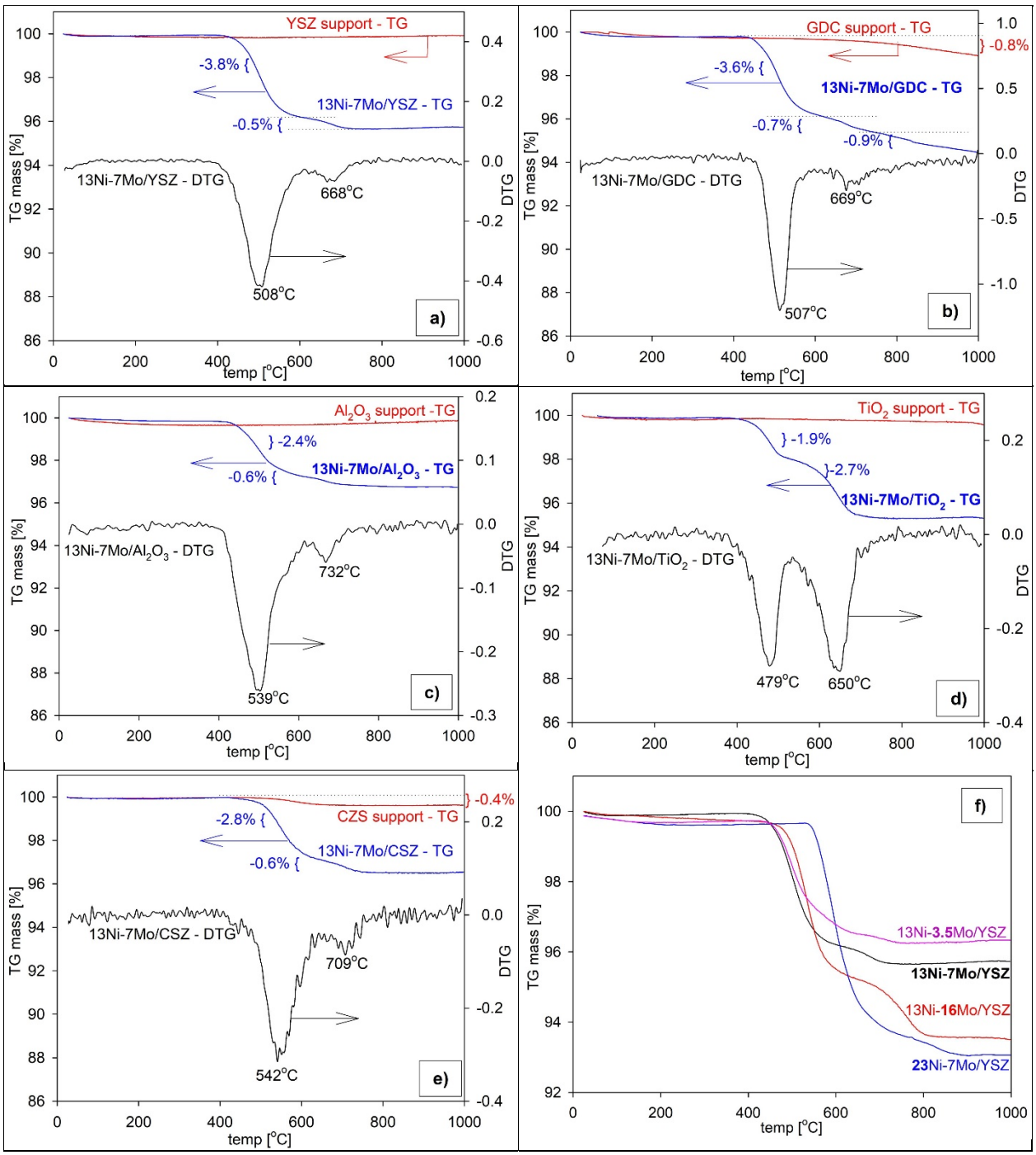

Fig. 1: TG and DTG curves of 13Ni-7Mo catalyst precursors; supported by: a) YSZ, b) GDC, c) Al_2O_3 and d) TiO_2, e) CSZ. f) TG curves of YSZ supported catalysts – various Ni-Mo compositions, 5%H_2/N_2.

Fig. 1f presents results from the reduction of YSZ supported catalysts with various Ni-Mo compositions. Modification to the Ni:Mo ratio changed the reduction behaviour. Increasing the loading of Mo increased the mass change during reduction owing to the higher metal oxide loading (Fig. 1f Mo: 3.5, 7 and 16%). Increasing Mo loading from 3.5 to 7% changed the mass reduction at around 450°C but did not affect the TGA at 650°C and above, though. This suggests that most Mo species are reduced at a temperature lower than 650°C,

The observed increase in the BET surface area suggested the formation of small particles. Increasing Mo loading to 16%, affected reduction at 650°C in the way of increasing the mass change. This suggested the formation of bulk Mo-Ni structures, which were more

difficult to reduce. This was confirmed by the decrease in the BET surface area. It was concluded that the co-deposition of Mo affected the interaction of Ni-Mo species with the YSZ support. This could be attributed to stronger integrating of Ni and Mo into the support and the formation of alloys. Increasing the amount of Ni from 13 to 23% increased the reduction temperature by around 50°C. The increase in reduction temperature after the increase in Mo or Ni loading suggested bulk effects and the formation of a solid solution with enhanced interaction with the surface. The decrease in the BET surface area suggested pore blocking and the formation of larger Ni-Mo particles.

The mass decrease of catalysts (13Ni-7Mo) during TPR was caused by the reduction of Ni-Mo oxides. However, the change of mass observed during the reduction process was smaller than expected for the used amount of Ni and Mo. This suggested that not all Ni and Mo were in the form of oxides after catalyst sintering and confirmed the formation of cermets reported in (Maluf and Assaf, 2009). Al_2O_3 supports were reported to form a spinel with Ni (Shen et al., 2019).

The conclusions from TPR analysis were further substantiated by XRD patterns of as-prepared and reduced catalysts. The crystal structure of prepared catalysts transformed during the reduction process. XRD characterisation of the sample oxide precursor of the Ni-Mo/Al_2O_3 catalyst comprised two groups of peaks (Fig. 2a). One group corresponded to the Al_2O_3 support (marked by squares) while another group could be indexed to the Ni-Mo oxides (all the peaks circled - Fig. 2a). All peaks circled blue for the as-prepared sample (Fig. 2b) could be attributed to $NiMoO_4$ and other oxide Ni-Mo forms formed during passivation. After reduction/carburisation, all diffractogram peaks related to the support remained unchanged with identical intensity, as is shown in the XRD pattern (Fig. 2b). All diffraction peaks related to Ni-Mo oxides disappeared and new peaks appeared related to Ni-Mo metal and Mo-C structures. This confirmed the complete reduction of Ni and Mo to the metallic form. A similar effect was observed for all the tested catalysts. The completed reduction should prevent coke deposition. It was reported that for Ni-Mo catalysts incomplete reduction/carburisation led to an increase in coke deposition during the reforming reaction (Hirose et al., 2011).

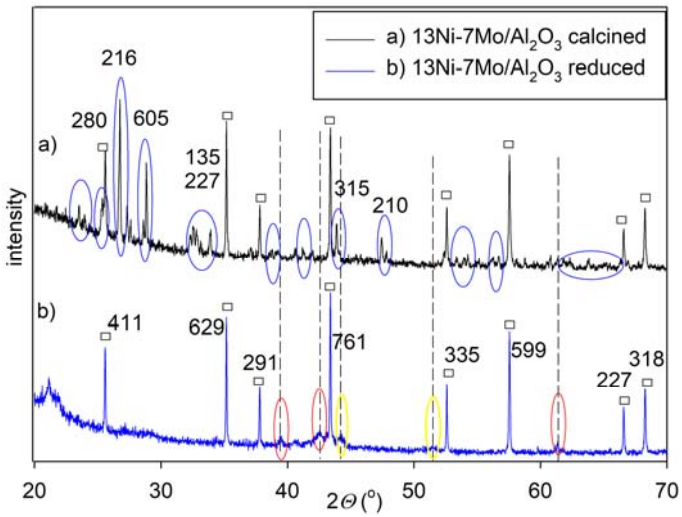

Fig. 2: XRD diffractograms of 13Ni-16Mo/Al_2O_3 catalyst: a) after calcination b) reduced.

2.4 Physicochemical characterisation - reduced catalysts

The Ni-Mo catalyst precursors synthesised by chemical precipitation were characterised by XRD analysis. Intensive peaks related to support material were marked respectively: (□) Al_2O_3, (■) GdO_3 (or GdO and CeO_2), (○)TiO_2, (●) MoO_2 (Fig. 3). Compared to the sharp, well-resolved peaks corresponding to support materials, all peaks relating to Mo-Ni crystallites were broader and much less intense, indicating a low crystallinity of the Ni and

Mo phases for all tested catalysts. The formation of broad diffraction peaks may suggest the formation of a solid solution. The small peaks at 2Θ 44.4, 51.8° are specific to metallic Ni. The peaks observed at 2Θ 44.4 were weak and wide and could be associated with Ni-Mo intermetallic/alloy compounds (NiMo, Ni_4Mo, Ni_3Mo, Ni_3Mo_3C and/or MoC), however, it could not be excluded that these might have related to carbon deposition during preparation. Carbon can sometimes deposit on the molybdenum carbide during carburisation (Ma et al., 2017; Yao et al., 2018). The most intense monometallic Ni related peak at 2Θ 51.8° was observed for the GDC support. No evidence of a monometallic Mo phase or molybdenum oxides was observed after catalyst reduction, implying an absence of Mo bulk crystal particles.

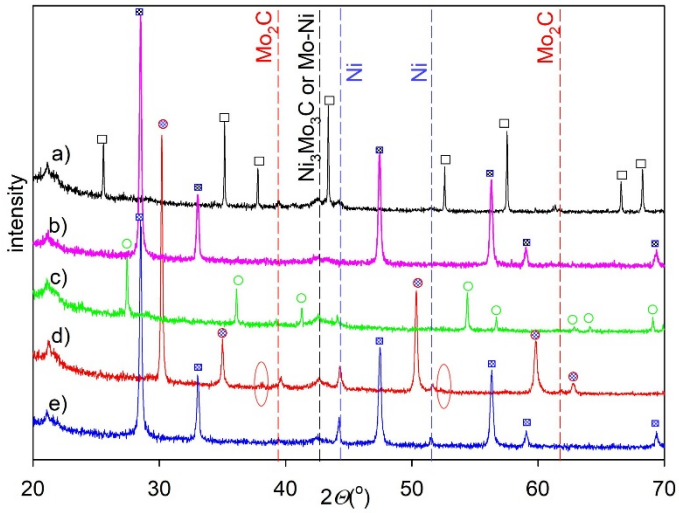

Fig. 3: XRD diffractograms of the reduced 13Ni-7Mo catalysts supported by: a) Al_2O_3, b) CSZ, c) TiO_2, d) YSZ, e) GDC.

The dissolution of the Mo phase into the Ni lattice and alloy formation can affect the lattice distortion and the formation of a mixture of NiMo, Ni_4Mo, or Ni_3Mo intermetallic phase (Hua et al., 2016a). Only residual carbide levels were observed by X-ray diffraction (XRD) after the synthesis. Molybdenum carbides have four crystal structures (α-MoC_{1-x}, β-Mo_2C, γ-MoC, and η-Mo_3C_2). The intensity of the obtained XRD diffractograms did not allow to unambiguously distinguish the obtained carbide form due to the low concentration of Mo and overlapping of the high-intensity signal from the support material. But they suggested that the selected synthesis conditions mostly led to the formation of β-Mo_2C. Diffraction peaks related to MoC were not detected. A highly amorphous and low-intensity phase attributed to Mo_2C with the characteristic XRD peak at 2Θ 39.8 was detected for all reduced Ni-Mo supported catalysts except GDC. The peaks were more intense for Al_2O_3 and YSZ supported catalysts. Additionally, for Al_2O_3 and YSZ supported catalysts, a peak was detected at 2Θ 61.9° that could be attributed to Mo_2C. For the YSZ supported catalyst, additional small peaks were detected at 2Θ 34.8° and 52.5° which could also be attributed to Mo_2C. If those two peaks were also present for the Al_2O_3 supported catalyst, they were overlapped by the intense peaks from the support material and were thus not detected.
The obtained results suggested that YSZ and Al_2O_3 promote the formation of a Mo-rich phase that is converted to Mo_2C during reduction/carburisation. Mo_2C is known to promote H_2 production (Ma et al., 2017). The low intensity of Ni related peaks suggested the formation of amorphous Ni structures, especially for the TiO_2 and CSZ supported catalysts. Peaks attributed to the Ni phase had a higher intensity for the GDC and YSZ supported catalysts, indicating higher crystallinity of the Ni, probably related to the formation of more agglomerated Ni-rich nanoparticles. The lack (or low concentration below the XRD detection sensitivity) of Mo_2C on TiO_2, GDC or CSZ supported catalysts

suggested high molybdenum oxide dispersion and strong interaction with the supports, which made it more difficult to convert to carbide.

3. YSZ supported Ni-Mo catalysts

From the tested Mo-Ni catalysts, the most promising for application in internal SOFC reforming appeared to be the YSZ supported catalyst. Therefore, this catalyst was further investigated. The aspect that was studied in more detail was the influence of Mo and Ni loading.

3.1 Materials Characterisation

With the increase in Mo concentration to 16% (and constant Ni 13%), the intensity of Mo_2C peaks decreased and simultaneously diffraction peaks related to Ni became less intensive (Fig. 4a). This is in agreement with the literature (Hirose et al., 2011), where an increase in Ni content for Ni:Mo catalysts enhanced the conversion of less active Mo-C structures into more active Mo_2C. The presence of Ni was reported to promote the carburisation process (Yao et al., 2018). The low intensity of Mo_2C peaks even at 16% Mo loading suggested a low Mo_2C ratio to total Mo species in the prepared catalysts. Peaks for MoO_2 were not detected. From XRD diffractograms for higher Ni loading (Fig. 4b - 23%Ni-7%Mo), it was observed that the intensity of Ni metal related diffraction peaks increased with increasing Ni loading. High intensity of Ni peaks suggested the formation of a Ni-rich phase.
Increase in nickel load resulted in a rise in crystallinity what was in agreement with the literature (Maluf and Assaf, 2009).(Maluf and Assaf, 2009). However, it slightly reduced the intensity of Mo_2C related peaks (compared to 13%Ni-7%Mo - Fig. 4c). This observation suggested that there was an optimal Ni:Mo ratio (close to 13%Ni-7%Mo) that promoted the Mo carburisation process for the YSZ supported catalyst. It can be deducted that Mo_2C as a catalyst requires doping of additional metal. Increasing Ni loading above 13% or changing the 7% Mo loading, both reduced Mo carburisation.

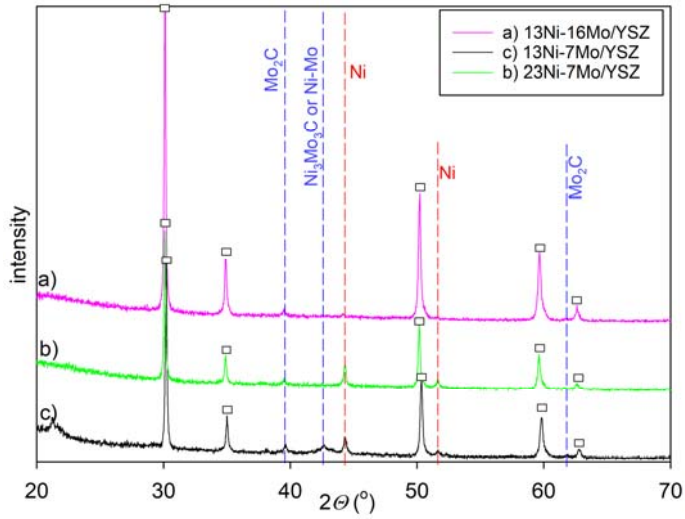

Fig. 4: XRD diffractograms of the Ni-Mo YSZ supported catalysts a) 13%Ni-16%Mo, b) 13%N-7%Mo, c) 23%Ni-7%Mo.

The material morphology was characterised by the SEM images of the synthesised Ni-Mo/YSZ catalyst. The catalyst precursor (Fig. 5B) exhibited various morphologies compared to the catalyst after heat treatment and reduction (Fig. 5A). After deposition, the Ni-Mo was homogeneously distributed on the YSZ structure in a mix of grains and flake-like shaped particles. The calcination followed by reduction/carburisation resulted in the formation of grains/crystals equally distributed on the YSZ surface. YSZ particles displayed

disorderly stacked, irregularly shaped particles in the size range of 0.5 to 2 µm, while Ni-Mo particles on the YSZ surface were spherical and 5 to 20 nm in size. The small size of the Ni-Mo particles could affect the XRD analysis and could be one of the reasons for the low intensity of the Ni-Mo diffraction peaks. The observed formation of Ni-Mo nanospheres was a promising tendency for the formation of good coke resistance and stable catalysts that could support internal SOFC reforming. The proven high dispersion of the catalyst confirmed the possibilities for the application of deposition-co-precipitation as a method to control the catalyst morphology under SOFC operating conditions. The obtained high dispersion maximised the exposition of active sites.

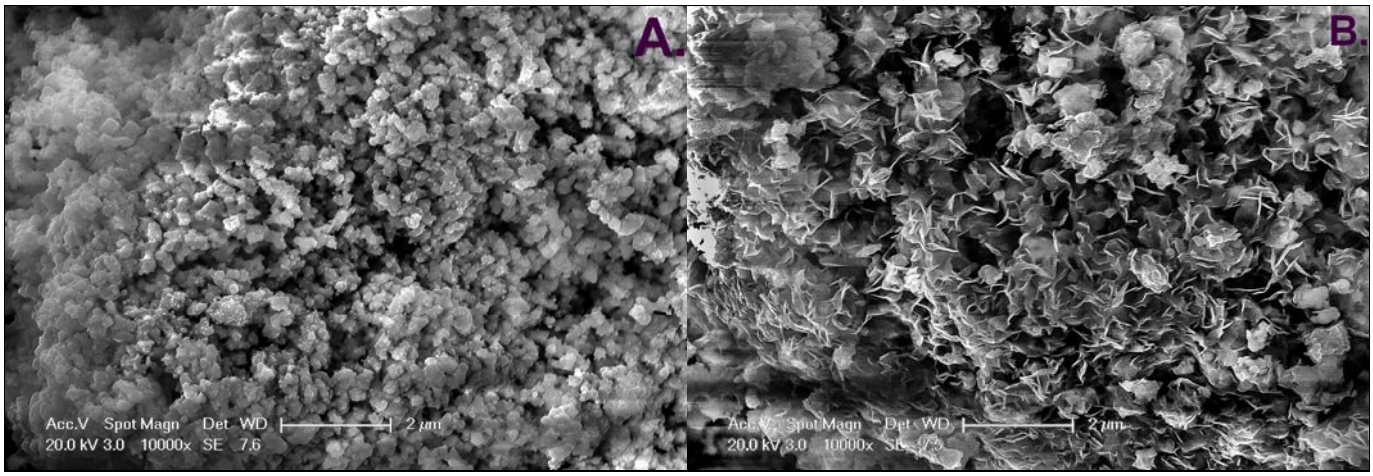

ig. 5: SEM images of 23%Ni-7%Mo/YSZ powder prepared using the deposition-co-precipitation method. A reduced, B after deposition.

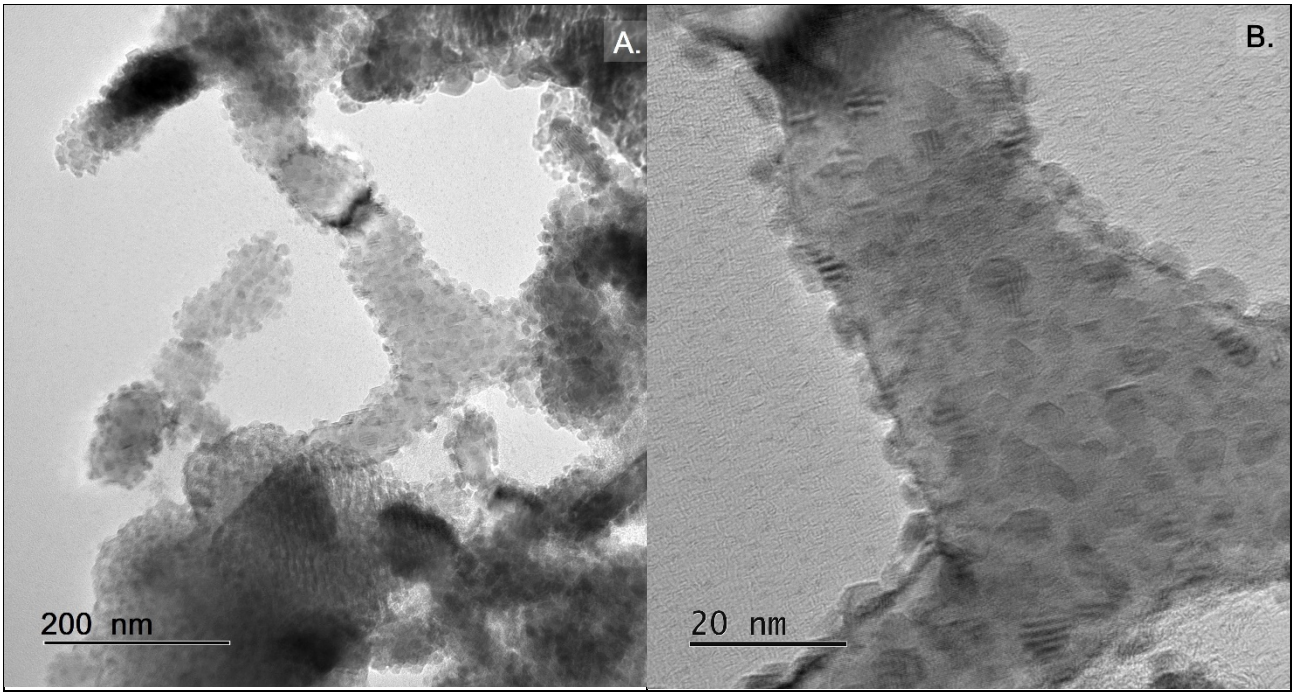

Fig. 6: TEM images of 23Ni-7Mo/YSZ reduced powder, prepared using the deposition-co-precipitation method.

TEM analysis was conducted to investigate the catalyst morphology. The micrographs of the reduced Ni-Mo/YSZ catalysts (Fig. 6) confirmed the observation of the formation of bimetallic Ni-Mo alloy nanospheres. Figs. 6A & B show that Ni-Mo nanoparticles were homogeneously dispersed on the YSZ support. Fig. 6B shows the periodically visible sets

of lattice fringes for the Ni-Mo phase. The high-resolution TEM revealed a petal-like structure of Ni-Mo nanocrystals. The lattice spacing was 0.8 to 1.1 nm in size. The EDS measurement confirmed that those small grains of 5 to 20 nm visible on the surface of bigger particles (Fig. 6) were Ni-Mo binary particles. Composition measurements underestimated the amount of segregation at a boundary caused by beam broadening due to the magnification used. The micrographs also showed that the Ni-Mo particles had a near-spherical shape and were well dispersed on the support surface. Unsupported Ni-Mo nanoparticles were not observed.
On SEM (Fig. 5) and TEM (Fig. 6) scans of the reduced catalyst, coke deposition was not detected. It has been reported that for some Mo catalysts the carburisation step can cause coke formation, which deactivates the catalyst (Ma et al., 2014).

3.2 Catalyst evaluation

The catalytic evaluation of synthesised Ni-Mo catalysts was carried out in a fixed-bed quartz micro-reactor (8 mm i.d. and 100 mm long) operated in a down-flow mode at atmospheric pressure. For the reforming reaction, 0.5 g of a supported catalyst (powder) was first diluted with SiC sand to a total volume of 2.5 cm^3 then placed in the centre of the reactor. Before the catalytic reaction, the Ni-Mo catalysts were reduced/carburised in situ in the reactor. Available in the literature data suggest that 700°C is sufficient for the carburisation/reduction process of similar samples (Ma et al., 2017; Reddy et al., 2019; Yao et al., 2018). However, the TPR tests (Fig.1) indicated that for the complete reduction of the tested catalysts required was around 750°C (in 5%H_2/N_2). Therefore, the tested catalysts were reduced and simultaneously carburised at 750°C for 1 hour in a gas mixture of H_2:CH_4:N_2 with the ratio of 50:25:25 ml min^{-1}. The quality of the reduction process was confirmed by XRD results (Fig.3 and 4). The catalyst was passivated by flowing N_2 into the tube for 15 min at the reaction temperature. The reforming reaction of simulated biogas with steam in combined steam and dry reforming was conducted at temperatures 650, 700, 750 and 800°C. The CH_4:CO_2:H_2O molar ratio was 1:0.5:1 for combined steam and dry reforming, and the ratio CH_4:CO_2 was set to 1:1 for dry reforming, with a CH_4 flow rate of 50 or 25 ml min^{-1}. The effluent was cooled by passing through an ice trap where eventual liquid products were condensed. An on-line GC was used for quantitative and qualitative analysis of reaction products. CH_4 and CO_2 conversions were calculated from a comparison of the molar concentration of CH_4 and CO_2 at reactor inlet and outlet. For the CO_2, it was a net conversion that included eventual CO_2 generation from reforming reactions.
All five tested catalysts were stable during the 4 hours of reaction test (Fig. 7). However, the TiO_2 supported catalyst showed some degradation during the first 2 hours and stabilised after that.

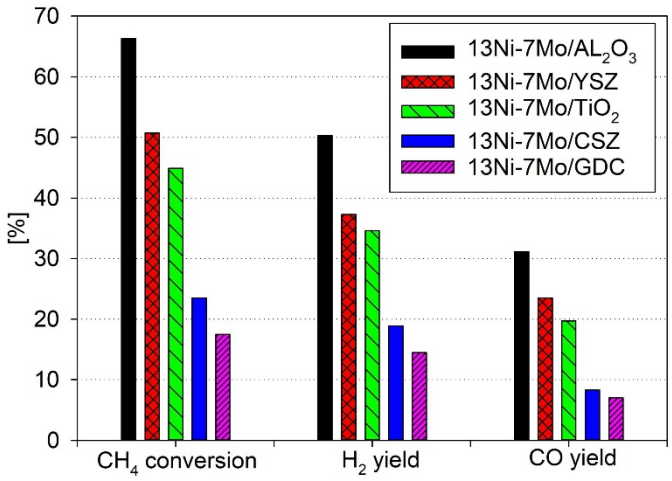

Fig. 7: Catalyst performance (average from 4 h reaction); 750°C, 0.5 g catalyst, CH_4:CO_2:H_2O 1:0.5:1, CH_4 flow 50 ml·min^{-1}.

The obtained results indicated that the support material strongly influenced the catalyst performance for biogas steam reforming. For the 13Ni-7Mo catalysts, the performance according to the support materials was observed in the sequence Al_2O_3 > YSZ > TiO_2 > CSZ > GDC. A very similar order of support materials was reported in the literature (Ma et al., 2017) for Mo_2C catalysts in dry reforming or Ni-based catalysts in combined steam and dry reforming (Okutan et al., 2020). The difference can be attributed to distinct interactions between the tested supports and the NiO-MoO_3 bulk from catalyst preparation. Additionally, TGA results (Fig. 1) suggested that there was an interaction of the support with the Ni-Mo precursors and the formation of a composite phase. The mass decrease during catalyst reduction was much lower than expected from the Ni and Mo loading. The higher activity of Al_2O_3 and YSZ supported catalysts for methane conversion can be explained by the formation of molybdenum carbide, as confirmed by XRD analysis. Transition metal carbides have higher activity compared to their parent metals due to the modification of electronic properties by introducing carbon that affects the binding energy (Porosoff et al., 2014). The highest H_2 and CO selectivity were obtained for Al_2O_3, and YSZ supported catalysts. The observed CH_4 conversion was similar to the reported in the literature for Ni (Okutan et al., 2020) or Ni/Co (Al-Fatesh et al., 2018) based catalysts. Relatively low CO yield (for example, 30% for the 13Ni7Mo/Al_2O_3 catalyst) and high CH_4 conversion (over 65%) suggested that part of the CO produced in the reforming reaction was converted to CO_2 in the water-gas shift reaction.

The support material affected the activity of the tested catalysts. However, the relative proportion between CH_4 conversion and yields of H_2 and CO remained unchanged. It was concluded that the support material affected the intensity of reforming reactions but did not affect the nature of those reactions. The influence of catalyst support on selectivity was insignificant under the tested conditions. The H_2:CO ratio in the produced syngas was high for all the catalysts; 5 for Al_2O_3 and YSZ supported catalysts and 6 to 7 for GDC and CSZ supported catalysts.

For all the tested catalysts, only steam reforming occurred during the combined steam and dry reforming of CH_4. The CO_2 concentration in syngas produced for all the catalysts was higher than the amount of CO_2 in simulated biogas before reforming. If some CO_2 took part in reforming, it was offset by the CO_2 produced from steam reforming. The amount of CO_2 in produced syngas was by 10-40% higher than in the feedstock (biogas). It can be concluded that synthesized catalysts are effective in methane steam reforming, but do not support dry reforming reaction in combined CH_4 reforming. The competition between the reactions of steam and dry reforming in the combined reforming was so high that only steam reforming occurred in the situation when the amount of steam was higher than CO_2 (CH_4:CO_2:H_2O 1:0.5:1).

The tested catalyst had lower performance compared with a commercial catalyst HiFUEL^{TM} R110 (Alfa Aesar) at the tested conditions, The HiFUEL^{TM} R110, a catalyst tailored for steam reforming, resulted in 99% CH_4 conversion at the tested conditions. The close to equilibrium CH_4 conversion was also reported for Al supported catalysts at similar conditions (Koo et al., 2009). Therefore, the tested catalysts require some microstructure improvements for application as an external reforming catalyst.

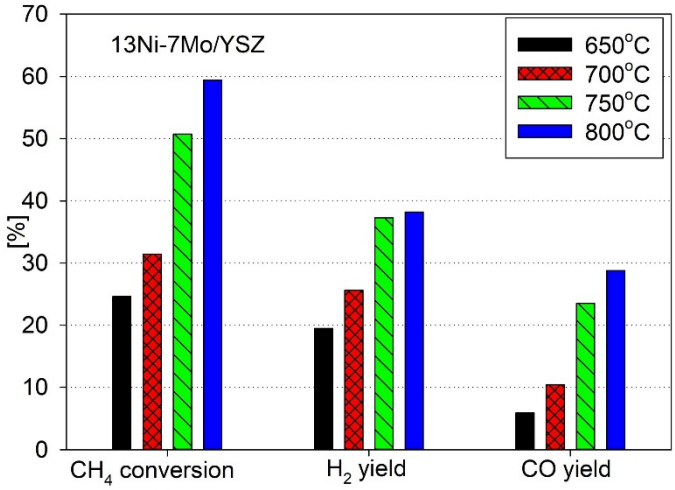

Fig. 8: 13Ni-7Mo/YSZ catalyst performance at various reaction temperatures (average from 4 h reaction). CH_4:CO_2:H_2O molar ratio 1:0.5:1, catalyst 0.5 g, CH_4 gas-in flow 50 ml·min^{-1}.

Increasing the reaction temperature from 750°C to 800°C resulted in an improvement in CH_4 conversion by 10%, simultaneously improving CO yield and slightly also H_2 yield (Fig. 8). The complete conversion was not achieved even at 800°C. Elevated temperature shifted the water-gas shift reaction to CO and H_2O production and promoted dry reforming.

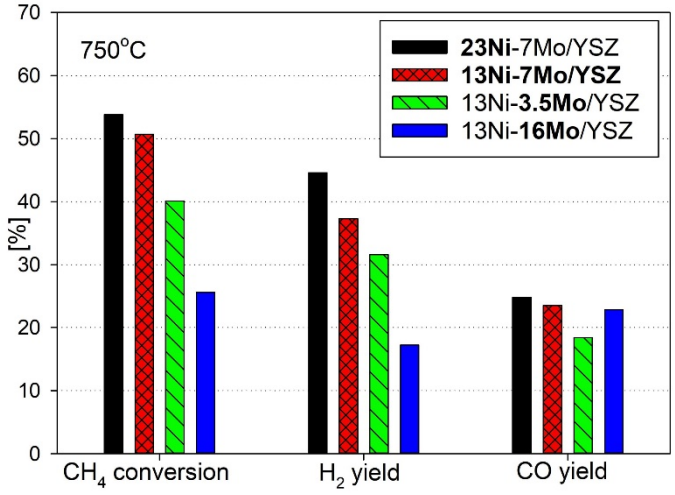

Fig. 9: Catalyst performance (average from 4 h reaction); 750°C, 0.5 g of catalyst, CH_4:CO_2:H_2O molar ratio 1:0.5:1, CH_4 flow 50 ml·min^{-1}.

Increasing Ni content improved catalyst performance for combined CH_4 reforming. It can be assumed that the rise in Ni content increased the formation of the Ni-rich phase, which enriched catalyst activity by promoting CH_4 dissociation. Higher Ni content significantly improved H_2 yield and slightly increased CO yield. This suggested that the Ni-rich phase promoted the water-gas shift reaction (CO_2 and H_2 production). Under constant 13%Ni loading, the highest catalyst activity was obtained for a Ni:Mo mass ratio of 13%:7%. Both, increasing Mo content to 16% or reducing to 3.5%, decreased the catalyst activity. This can be related to the decrease in Mo_2C concentration observed by XRD (Fig. 4) and to the lower surface area observed by BET analysis (Table 1) for high 16% or low 3.5% Mo loading. Covering of $Ni^{(0)}$ particles by MnO_x was reported as the reason for the lower activity of the catalysts with higher Mo loading (Claude et al., 2020). Increasing Mo content from 13Ni7Mo to 13Ni16Mo reduced CH_4 conversion and H_2 yield, but increased CO yield. This suggests that Mo can promote reverse water-gas shift reaction (CO_2+H_2→H_2O +CO).

It was also reported that the formation of $MoNi_4$ species with the increase in Mo loading reduces catalyst activity (Yao et al., 2017). For the tested catalyst, this was impossible to verify due to the low crystallinity of the Ni-Mo structures. For comparison, Shi's et al. (Shi et al., 2012) studies on Ni-Mo_2-C catalysts (unsupported) observed that for dry reforming the optimal Ni:Mo ratio was identified as 1:2. They also suggested that higher Mo content resulted in catalyst deactivation due to bulk oxidation by CO_2.

High catalyst stability is another crucial parameter of catalyst performance. A time-stream stability study was carried out for 100 hours using the biogas steam reforming reaction and 45 hours for dry CH_4 reforming to confirm catalyst stability. Fig. 10 displays the performance of the 23Ni7MoYSZ catalyst for methane combined steam and dry reforming over time.

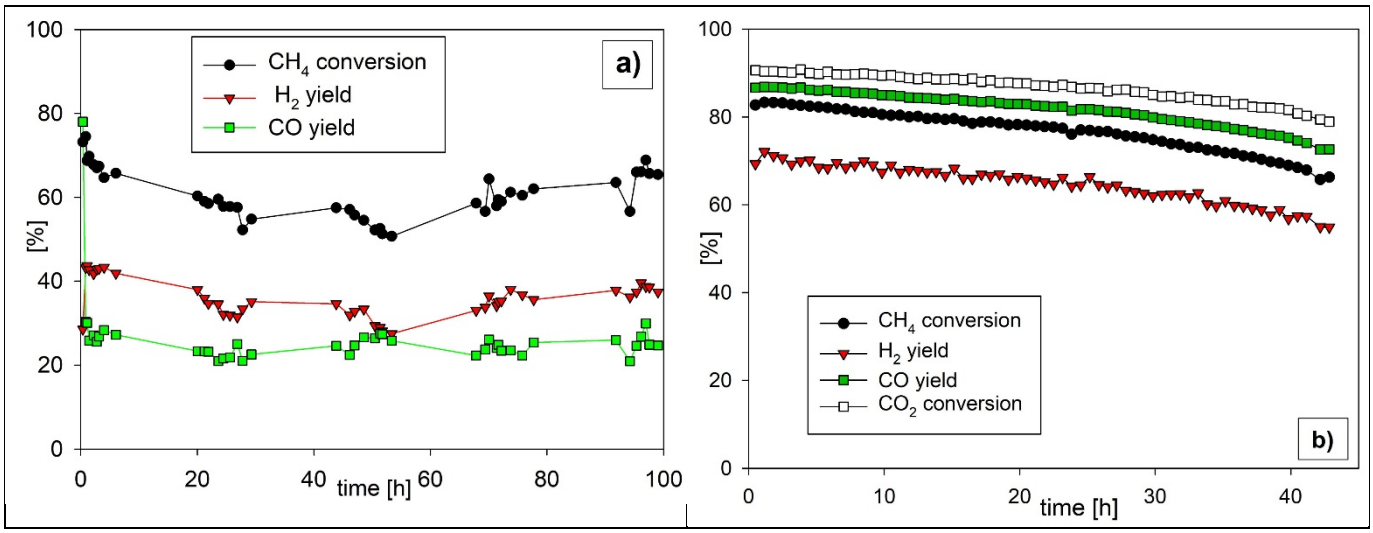

Fig. 10: 23Ni-7Mo/YSZ catalyst performance over time, at 750°C, catalyst 0.5 g, CH_4 flow 50 ml·min^{-1}; A) CH_4:CO_2:H_2O molar ratio 1:0.5:1, B) CH_4:CO_2:molar ratio 1:1.

The Ni-Mo/YSZ catalyst showed better stability in CH_4 combined reforming without obvious degradation in the catalyst activity, during the stability test at 750°C. The composition of the outlet gas was stable during the 100 hours experiment. The main product of the methane combined steam and dry reforming was H_2 (over 55% in produced syngas - dry) with over 20% of CO_2 and remaining CH_4 with lower CO concentration. The reforming results showed that the 23Ni-7Mo/YSZ catalyst showed high and stable catalytic activity for CH_4 combined reforming at 750°C and might be suitable for application in direct hydrocarbon, internal reforming SOFC systems. The product selectivity did not change during the testing time. The small initial decrease in CH_4 conversion could be attributed to sintering rather than carbon deposition, since no apparent carbon structures (fibres, beds) appeared on SEM scans after the 100-hour test in humidified biogas. The origin of the slight increase in CH_4 conversion after 6070 hours of reforming is not clear. Is it possible that C adsorption promoted MoC_2 formation that improved catalytic activity for steam reforming. However, the increase in MoC_2 was not confirmed. Possible is also that part of the initially deposited coke was oxidised or changed structure.
With the CH_4:H_2O molar ratio of 1:1 the relatively high water content promoted the water-gas shift reaction (in the gas feed, which resulted in low CO yield. This catalyst property could make this catalyst suitable for efficient H_2 generation via water-gas shift reaction (Nagai et al., 2006).
The gradual internal combined steam and dry reforming of hydrocarbons is an interesting option for SOFC (Yin and Chuang, 2017). The nature of the process changes along the cell with the increase in steam generation during cell operation. SOFC systems with anode

gas recirculation (with a water trap) can provide CO_2 for gradual internal reforming with dry reforming at the cell inlet, followed by combined steam and dry reforming. Therefore, the prepared 23Ni7Mo/YSZ catalyst was tested also for methane dry reforming.
The obtained CH_4 conversion of around 80% and CO_2 conversion of around 90% was relatively high at a reaction temperature of 750°C (low for dry reforming). Continuous slow degradation was observed during the tested 45 hours. CH_4 conversion subsequently decreased to around 70%. This degradation was mainly caused by coke deposition rather than particle agglomeration or Mo_2C oxidation. However, for Ni-Mo catalysts with high Mo_2C concentration, some deactivation was possible due to Mo_2C bulk oxidation by oxygen from CO_2 dissociation (Shi et al., 2012). The obtained CH_4 conversion was higher than for the reported Ni-Mo/Al_2O_3 catalysts (with the much higher surface area) obtained from wet impregnation (Yao et al., 2017).
The carbon tolerance behaviour of the prepared catalysts was analysed by comparing temperature-programmed TGA analysis of samples after 4 hours of reforming reaction. The results showed differences in the kinetics of coke deposition for the tested catalysts. Table 2 presents the TGA analyses of the tested Ni-Mo supported catalysts after the 4 hours of combined steam and dry reforming (presented in Figs. 7 to 10). The obtained TGA results showed carbon tolerance of each cermet and present the inhibition of carbon deposition through reaction temperature and Ni-Mo nominal loading.

Table 3: Coke deposition after 4 h of reaction - CH_4:CO_2:H_2O 1:0.5:1, at 750°C, catalyst 0.5 g, CH_4 50 ml·min^{-1}.

Catalyst No	Catalyst	Reaction [°C]	Coke [mg·g_{cat}^{-1}]
1	13Ni-7Mo/YSZ	800	2.1
1	13Ni-7Mo/YSZ	750	2.5
1	13Ni-7Mo/YSZ	700	6.1
1	13Ni-7Mo/YSZ	650	8.6
2	13Ni-7Mo/GDC	750	0
3	13Ni-7Mo/Al_2O_3	750	2.0
4	13Ni-7Mo/TiO_2	750	303.4
5	13Ni-7Mo/CSZ	750	17.3
6	23Ni-7Mo/YSZ	750	8.6
7	13Ni-3.5Mo/YSZ	750	137.9
8	13Ni-16Mo/YSZ	750	0
Dry reforming (CH_4:CO_2 1:1)			
1	13Ni-7Mo/YSZ	750	88.4

The reduction in coke deposition on the YSZ supported Ni-Mo catalyst was ascribed to the molybdenum component. The increase in Mo content improved the resistance to carbon deposition. The increase in Mo loading from 3.5 to 7 and 16% (XRF) led to reduced coke deposition from 137.9 to 2.5 and 0 mg·g_{cat}^{-1}, respectively. The inhibition properties of Mo have previously been reported in the literature (Hirose et al., 2011; Hua et al., 2016a; Niakolas et al., 2013; Niakolas et al., 2011). Bkour et al. (Bkour et al., 2020) explained the lower coke deposition for Mo doped Ni catalysts by the fact that in the Ni(111) the d-band centre of the Ni atom for the Ni 3d orbital which is in close proximity to the Mo atom, shifts away from the Fermi level thus reducing the chances for electronic interaction between C and Ni. It was reported that additional improvement of Ni-Mo supported catalysts can be obtained by the addition of noble metals such as Au (Niakolas et al., 2011). It is worth to mention that the reaction time did not affect the coke deposition. The mass of coke deposited after the 100 hour reaction (Fig. 10 A) was the same as after 4 hours. This suggested a steady-state of carbon deposition after the first few hours of reaction, with a close to zero carbon deposition rate in the following period of time. An increase in reaction

temperature reduced coke deposition from 8.6 mg·g_{cat}^{-1} at 650°C to 2.1 mg·g_{cat}^{-1} at 800°C. The increase in reaction temperature also changed the structure of the deposited coke, making it more graphitic.

The resistance of supported 13Ni-7Mo catalysts to coke deposition under combined CH_4 reforming according to support was GDC > Al_2O_3 > YSZ > CSZ > TiO_2. In agreement with the above discussion, TGA results showed that the 13Ni-7Mo/GDC cermet was a good candidate for reforming systems concerning carbon deposition, with no coke formation after 4 hours of reaction. The Ni-Mo/GDC structure has been previously reported to be resistant to coke deposition (Papaefthimiou et al., 2013). The authors suggested that the carbon tolerance of a Ni-GDC structure was partially related to the reduced ceria which activates oxygen species that are highly reactive with adsorbed CH_x and promote CO and H_2 formation. Nevertheless, the GDC supported catalyst showed the worst CH_4 conversion and H_2 yield under the tested conditions in this study.

The TiO_2 supported catalyst was prone to coke deposition, with over 300 mg g_{cat}^{-1} of carbon deposited after the 4-hour reaction. A high coke deposition of 88.4 mg g_{cat}^{-1} was also observed after the dry reforming test, despite the higher catalyst activity. This was the main reason for the catalyst deactivation during long-term dry reforming evaluation (Fig 10B).

The performance of the tested catalysts was below commercial state-of-the-art reforming catalysts (HiFUEL^{TM} R110 – results not presented). However, it should be pointed out that the tested catalysts were produced using low porosity supports. The tested materials YSZ, GDC and CSZ are used for the production of dense electrolytes and for production of anodes where porosity is obtained by Ni reduction or by adding porosity agents during fabrication.

The potential application of the YSZ, GDC and CSZ supported Ni-Mo catalysts is for the SOFC anode supporting layer where most of the CH_4 reforming reaction takes place. Those coke resistant catalysts can be used for electrodes designed for direct internal reforming of hydrocarbons or for direct utilisation where some CO_2 or H_2O is added to the fuel (like biogas or partially externally reformed hydrocarbons). Additionally, the performance of these catalysts is expected to increase during the cell operation due to the support material oxygen ions transport properties. From the tested catalyst, the most promising for the application in combined internal reforming of CH_4 was the 13Ni-7Mo/YSZ.

4. Summary

Supported Ni-Mo catalysts were synthesised using the deposition-co-precipitation method. The variety of supports and the molar ratio of Ni:Mo led to a variety of morphologies, reduction temperatures, and reforming activities. The optimum Ni:Mo ratio that promoted the Mo carburisation process for the YSZ supported catalyst was 13%Ni:7%Mo. Reduced Ni-Mo catalysts showed the typical XRD peaks of amorphous Ni and MoC_2 was detected on the Ni-Mo catalysts supported by YSZ and Al_2O_3.

This preparation method could result in the formation of more effective and cheaper SOFC anodes, however, there are still many parameters requiring consideration in order to understand the process with SOFC experiments. Prepared Ni-Mo catalysts supported by YSZ, GDC and CSZ with improved carbon tolerance have the potential to be used as anodes in SOFC. Those catalyst supports were compared to typical reforming supports Al_2O_3 and TiO_2. Further investigation is currently underway in the process to evaluate the properties of the described materials and their application as SOFC anodes.

Ni-Mo supported catalysts were studied for combined steam and dry reforming of methane and for methane dry reforming. The selection of support material significantly affected Ni-Mo catalyst reaction kinetics and yields of desirable products of H_2 and CO during the CH_4 combined (steam-dry) reforming. For five catalysts prepared using the deposition-co-

precipitation of Ni (13%) and Mo (7%) on ceramic supports, the most active were those where the formation of Mo_2C was detected. From the studied catalysts, the 13Ni-7Mo/YSZ sample showed the best combination of results with structural and physicochemical properties, activity and selectivity to H_2 and CO, and resistance to carbon deposition. The Ni-Mo/ catalysts with low molybdenum content presented a better catalytic performance for the methane reforming, however, the higher Mo content significantly improved resistance to solid carbon formation.

Acknowledgements
The results are part of the outcome of the "Biogas to energy - catalyst for biogas combined steam/dry reforming" project funded under EPSRC/University of Birmingham Global Challenges Research Fund: 1516GCRF018 and EPSRC JUICED Hub EP/R023662/1.

Reference List

Al-Fatesh, A., Singh, S.K., Kanade, G.S., Atia, H., Fakeeha, A.H., Ibrahim, A.A., El-Toni, A.M., Labhasetwar, N.K., 2018. Rh promoted and ZrO2/Al2O3 supported Ni/Co based catalysts: High activity for CO2 reforming, steam–CO2 reforming and oxy–CO2 reforming of CH4. International Journal of Hydrogen Energy 43, 12069-12080.
Asset, T., Roy, A., Sakamoto, T., Padilla, M., Matanovic, I., Artyushkova, K., Serov, A., Maillard, F., Chatenet, M., Asazawa, K., Tanaka, H., Atanassov, P., 2016. Highly active and selective nickel molybdenum catalysts for direct hydrazine fuel cell. Electrochimica Acta 215, 420-426.
Behnejad, B., Abdouss, M., Tavasoli, A., 2019. Comparison of performance of Ni–Mo/γ-alumina catalyst in HDS and HDN reactions of main distillate fractions. Petroleum Science 16, 645-656.
Bkour, Q., Che, F., Lee, K.-M., Zhou, C., Akter, N., Boscoboinik, J.A., Zhao, K., Gray, J.T., Saunders, S.R., Grant Norton, M., McEwen, J.-S., Kim, T., Ha, S., 2020. Enhancing the partial oxidation of gasoline with Mo-doped Ni catalysts for SOFC applications: An integrated experimental and DFT study. Applied Catalysis B: Environmental 266, 118626.
Claude, V., Mahy, J.G., Tilkin, R.G., Lambert, S.D., 2020. Enhancement of the catalytic performances and lifetime of Ni/γ-Al2O3 catalysts for the steam toluene reforming via the combination of dopants: inspection of Cu, Co, Fe, Mn, and Mo species addition. Materials Today Chemistry 15, 100229.
Fang, M., Gao, W., Dong, G., Xia, Z., Yip, S., Qin, Y., Qu, Y., Ho, J.C., 2016. Hierarchical NiMo-based 3D electrocatalysts for highly-efficient hydrogen evolution in alkaline conditions. Nano Energy 27, 247-254.
Hirose, T., Ozawa, Y., Nagai, M., 2011. Preparation of a Nickel Molybdenum Carbide Catalyst and Its Activity in the Dry Reforming of Methane. Chinese Journal of Catalysis 32, 771-776.
Hua, B., Li, M., Zhang, Y.-Q., Chen, J., Sun, Y.-F., Yan, N., Li, J., Luo, J.-L., 2016a. Facile Synthesis of Highly Active and Robust Ni–Mo Bimetallic Electrocatalyst for Hydrocarbon Oxidation in Solid Oxide Fuel Cells. ACS Energy Letters 1, 225-230.
Hua, B., Yan, N., Li, M., Zhang, Y.Q., Sun, Y.F., Li, J., Etsell, T., Sarkar, P., Chuang, K., Luo, J.L., 2016b. Novel layered solid oxide fuel cells with multiple-twinned Ni0.8Co0.2 nanoparticles: The key to thermally independent CO2 utilization and power-chemical cogeneration. Energy and Environmental Science 9, 207-215.
Koo, K.Y., Roh, H.-S., Jung, U.H., Seo, D.J., Seo, Y.-S., Yoon, W.L., 2009. Combined H2O and CO2 reforming of CH4 over nano-sized Ni/MgO-Al2O3 catalysts for synthesis gas production for gas to liquid (GTL): Effect of Mg/Al mixed ratio on coke formation. Catalysis Today 146, 166-171.

Kundakovic, L., Flytzani-Stephanopoulos, M., 1998. Cu- and Ag-Modified Cerium Oxide Catalysts for Methane Oxidation. Journal of Catalysis 179, 203-221.
Lanzini, A., Leone, P., 2010. Experimental investigation of direct internal reforming of biogas in solid oxide fuel cells. International Journal of Hydrogen Energy 35, 2463-2476.
Lin, S.S.Y., Thomson, W.J., Hagensen, T.J., Ha, S.Y., 2007. Steam reforming of methanol using supported Mo2C catalysts. Applied Catalysis A: General 318, 121-127.
Liu, H., Liu, C., Yin, C., Chai, Y., Li, Y., Liu, D., Liu, B., Li, X., Wang, Y., Li, X., 2015. Preparation of highly active unsupported nickel–zinc–molybdenum catalysts for the hydrodesulfurization of dibenzothiophene. Applied Catalysis B: Environmental 174–175, 264-276.
Liu, H., Yin, C., Li, H., Liu, B., Li, X., Chai, Y., Li, Y., Liu, C., 2014. Synthesis, characterization and hydrodesulfurization properties of nickel–copper–molybdenum catalysts for the production of ultra-low sulfur diesel. Fuel 129, 138-146.
Ma, Y., Guan, G., Hao, X., Cao, J., Abudula, A., 2017. Molybdenum carbide as alternative catalyst for hydrogen production – A review. Renewable and Sustainable Energy Reviews 75, 1101-1129.
Ma, Y., Guan, G., Phanthong, P., Hao, X., Huang, W., Tsutsumi, A., Kusakabe, K., Abudula, A., 2014. Catalytic Activity and Stability of Nickel-Modified Molybdenum Carbide Catalysts for Steam Reforming of Methanol. The Journal of Physical Chemistry C 118, 9485-9496.
Majewski, A.J., Wood, J., Bujalski, W., 2013. Nickel–silica core@shell catalyst for methane reforming. International Journal of Hydrogen Energy 38, 14531-14541.
Maluf, S.S., Assaf, E.M., 2009. Ni catalysts with Mo promoter for methane steam reforming. Fuel 88, 1547-1553.
McIntosh, S., Vohs, J.M., Gorte, R.J., 2003. Effect of Precious-Metal Dopants on SOFC Anodes for Direct Utilization of Hydrocarbons. Electrochemical and Solid-State Letters 6, A240-A243.
McKone, J.R., Sadtler, B.F., Werlang, C.A., Lewis, N.S., Gray, H.B., 2013. Ni–Mo Nanopowders for Efficient Electrochemical Hydrogen Evolution. ACS Catalysis 3, 166-169.
Nagai, M., Zahidul, A.M., Matsuda, K., 2006. Nano-structured nickel–molybdenum carbide catalyst for low-temperature water-gas shift reaction. Applied Catalysis A: General 313, 137-145.
Niakolas, D.K., Athanasiou, M., Dracopoulos, V., Tsiaoussis, I., Bebelis, S., Neophytides, S.G., 2013. Study of the synergistic interaction between nickel, gold and molybdenum in novel modified NiO/GDC cermets, possible anode materials for CH4 fueled SOFCs. Applied Catalysis A: General 456, 223-232.
Niakolas, D.K., Athanasiou, M., Neophytides, S.G., Bebelis, S., 2011. Characterization and Carbon Tolerance of New Au - Mo - Ni/GDC Cermet Powders for use as Anode Materials in Methane Fuelled SOFCs. ECS Transactions 35, 1329-1336.
Okutan, C., Arbag, H., Yasyerli, N., Yasyerli, S., 2020. Catalytic activity of SBA-15 supported Ni catalyst in CH4 dry reforming: Effect of Al, Zr, and Ti co-impregnation and Al incorporation to SBA-15. International Journal of Hydrogen Energy 45, 13911-13928.
Papaefthimiou, V., Shishkin, M., Niakolas, D.K., Athanasiou, M., Law, Y.T., Arrigo, R., Teschner, D., Hävecker, M., Knop-Gericke, A., Schlögl, R., Ziegler, T., Neophytides, S.G., Zafeiratos, S., 2013. On the Active Surface State of Nickel-Ceria Solid Oxide Fuel Cell Anodes During Methane Electrooxidation. Advanced Energy Materials 3, 762-769.
Porosoff, M.D., Yang, X., Boscoboinik, J.A., Chen, J.G., 2014. Molybdenum Carbide as Alternative Catalysts to Precious Metals for Highly Selective Reduction of CO2 to CO. Angewandte Chemie International Edition 53, 6705-6709.
Reddy, K.P., Dama, S., Mhamane, N.B., Ghosalya, M.K., Raja, T., Satyanarayana, C.V., Gopinath, C.S., 2019. Molybdenum carbide catalyst for the reduction of CO2 to CO:

surface science aspects by NAPPES and catalysis studies. Dalton Transactions 48, 12199-12209.
Rismanchian, A., Mirzababaei, J., Chuang, S.S.C., 2015. Electroless plated Cu-Ni anode catalyst for natural gas solid oxide fuel cells. Catalysis Today 245, 79-85.
Sehested, J., Jacobsen, C.J.H., Rokni, S., Rostrup-Nielsen, J.R., 2001. Activity and Stability of Molybdenum Carbide as a Catalyst for CO2 Reforming. Journal of Catalysis 201, 206-212.
Shen, Z., Ke, M., Lan, L., He, P., Liang, S., Zhang, J., Song, H., 2019. Active phases and reaction performance of Mo improved Ni/Al2O3 catalysts for thioetherification. Fuel 236, 525-534.
Shi, C., Zhang, A., Li, X., Zhang, S., Zhu, A., Ma, Y., Au, C., 2012. Ni-modified Mo2C catalysts for methane dry reforming. Applied Catalysis A: General 431-432, 164-170.
Troskialina, L., Dhir, A., Steinberger-Wilckens, R., 2015. Improved Performance and Durability of Anode Supported SOFC Operating on Biogas. ECS Transactions 68, 2503-2513.
Wang, Y., Woodward, C., Zhou, S.H., Liu, Z.K., Chen, L.Q., 2005. Structural stability of Ni–Mo compounds from first-principles calculations. Scripta Materialia 52, 17-20.
Xiong, K., Li, L., Zhang, L., Ding, W., Peng, L., Wang, Y., Chen, S., Tan, S., Wei, Z., 2015. Ni-doped Mo2C nanowires supported on Ni foam as a binder-free electrode for enhancing the hydrogen evolution performance. Journal of Materials Chemistry A 3, 1863-1867.
Yao, L., Galvez, M.E., Hu, C., Da Costa, P., 2017. Mo-promoted Ni/Al2O3 catalyst for dry reforming of methane. International Journal of Hydrogen Energy 42, 23500-23507.
Yao, L., Wang, Y., Galvez, M.E., Hu, C., Da Costa, P., 2018. Ni–Mo2C supported on alumina as a substitute for Ni–Mo reduced catalysts supported on alumina material for dry reforming of methane. Comptes Rendus Chimie 21, 247-252.
Yin, W., Chuang, S.S.C., 2017. CH4 internal dry reforming over a Ni/YSZ/ScSZ anode catalyst in a SOFC: A transient kinetic study. Catalysis Communications 102, 62-66.